Modeling methane emissions from the Alaskan Yukon River basin, 1986–2005, by coupling a large-scale hydrological model and a process-based methane model

Xiaoliang Lu[1] and Qianlai Zhuang[1,2]

Received 25 August 2011; revised 14 February 2012; accepted 18 February 2012; published 19 April 2012.

[1] Much progress has been made in methane modeling for the Arctic. However, there is still large uncertainty in emissions estimates due to the spatial variability in water table depth resulting from complex topographic gradients, and due to variations in methane production and oxidation due to complex freezing and thawing processes. Here we extended an extant methane emission module within a biogeochemistry model, the Terrestrial Ecosystem Model (TEM), to include a large-scale hydrology model, the variable infiltration capacity (VIC) model. The VIC model provides the required inputs, including freezing and thawing fronts, soil temperature and moisture, to the methane module. The effect of topography on the redistribution of soil moisture and water table depth was explicitly modeled using the TOPMODEL approach. The coupled modeling framework was applied to the Yukon River basin at a spatial resolution of 1 km from 1986 to 2005. The simulations show that the average annual net emissions of CH_4 from the region are 4.01 Tg CH_4 yr^{-1}. El Niño phenomena usually lead to positive emission anomalies, while decreases in net CH_4 emissions may be associated with strong La Niña events. Precipitation was found to be more closely related to CH_4 dynamics than to soil temperature and active layer depth during the study period. This study suggests that the effects of soil freezing and thawing processes and the effects of microtopography on hydrology should be considered in the quantification of CH_4 emissions.

Citation: Lu, X., and Q. Zhuang (2012), Modeling methane emissions from the Alaskan Yukon River basin, 1986–2005, by coupling a large-scale hydrological model and a process-based methane model, *J. Geophys. Res.*, *117*, G02010, doi:10.1029/2011JG001843.

1. Introduction

[2] Methane (CH_4), a greenhouse gas, has a much larger radiative forcing potential than CO_2, and wetlands are the largest natural source of CH_4 to the atmosphere, accounting for 25% of the global total annual emissions [*Intergovernmental Panel on Climate Change*, 2007]. The high northern latitudes contain more than 40% of the global wetlands [*Matthews and Fung*, 1987, *Aselmann and Crutzen*, 1989]. In arctic regions, relatively low soil temperatures, water saturation and hypoxia can drastically reduce microbial respiration rates, leading to an accumulation of soil organic matter. With warming and thawing permafrost, a large amount of CH_4 emissions from the soils and permafrost have been observed [e.g., *Khvorostyanov et al.*, 2008].

[3] *Zhuang et al.* [2004] coupled the Terrestrial Ecosystem Model (TEM) and a soil thermal model [*Zhuang et al.*, 2001, 2003a, 2003b] with a methane model to simulate methane emissions from northern high latitudes. However, there are at least four major uncertainty factors in quantifying CH_4 budgets in arctic regions. First, wetland extent varies seasonally and annually. Most modeling studies used static wetland data sets [e.g., *Matthews and Fung*, 1987] with the assumption that wetland area is constant during a study period. At present, remote sensing makes it possible to observe seasonally varying inundation extent. For example, optical sensors [*Prigent et al.*, 2007] and synthetic aperture radar (SAR) [*Melack et al.*, 2004; *Papa et al.*, 2006] were used to identify inundation area changes. However, optical remote sensing is frequently impeded by cloud or vegetation cover. Alternatively, passive and active microwave systems have better ability to penetrate cloud and vegetation cover, while they usually suffer from data unavailability, especially high time-resolution data for large spatial coverage. In any case, model capability to characterize wetland inundation dynamics is needed for quantifying methane emissions. Second, existing modeling studies lack of suitable schemes to quantify the effects of spatial heterogeneity on water table depth (WTD), which may

[1]Department of Earth and Atmospheric Sciences, Purdue University, West Lafayette, Indiana, USA.
[2]Department of Agronomy, Purdue University, West Lafayette, Indiana, USA.

0148-0227/12/2011JG001843

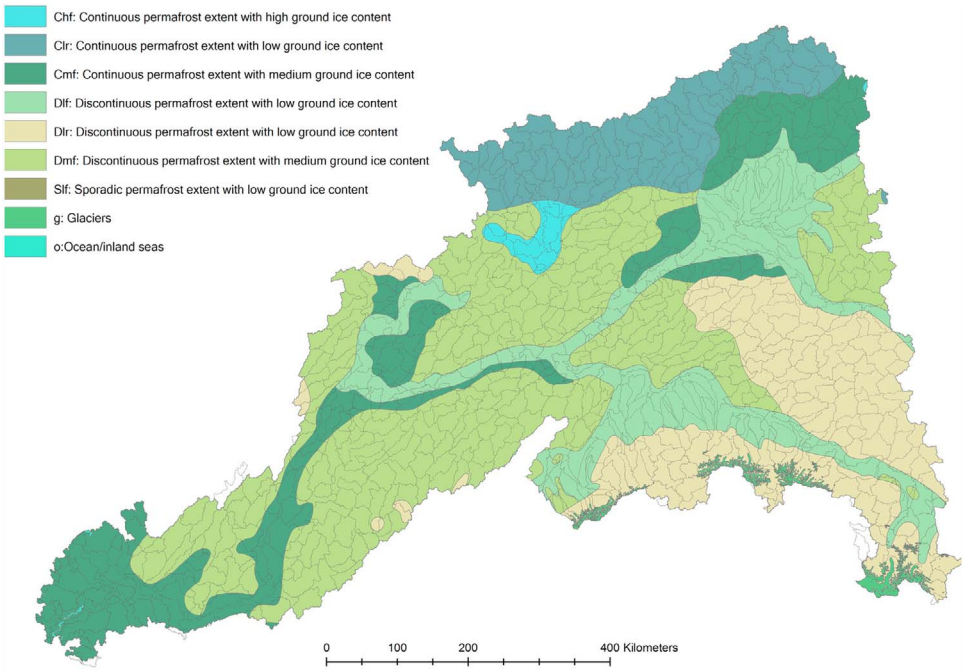

Figure 1. Distribution of permafrost and ground-ice conditions in the Yukon River basin. The HUC10 watershed boundary is indicated with black solid lines.

result in systematic biases in large-scale estimates of wetland methane emissions [*Bohn and Lettenmaier*, 2010]. Water table depth calculated by hydrological models is usually assumed equally distributed in each grid cell of the landscape. This simple treatment of water table depth neglects the effects of microtopography on water table dynamics [e.g., *Walter et al.*, 2001; *Zhuang et al.*, 2004], to which methane production and oxidation process is sensitive [*Zhuang et al.*, 2007]. A scheme to take sub-grid variations in topography into account should improve the methane emission modeling [*Bohn et al.*, 2007; *Bohn and Lettenmaier*, 2010]. Third, there are complex freezing and thawing processes in the Arctic [*Mastepanov et al.*, 2008, *O'Connor et al.*, 2010] including seasonal variations in active layer depth (ALD) due to ice thawing and upward/downward freezing, which change boundaries between oxidation and production zones in soil profiles. A methane model applied in arctic regions should adequately consider soils thermal effects. Finally, the original model used a fixed threshold (500 μmol) for estimating methane ebullition, while a dynamic threshold that relates to water table location (hydrostatic pressure) and soil temperature should be considered [e.g., *Wania et al.*, 2010].

[4] Here we conducted a study by incorporating a variable infiltration capacity (VIC) model into our existing methane model [*Zhuang et al.*, 2004] to improve the quantification of daily CH_4 fluxes from the Yukon River basin from 1986 to 2005. The effects of freeze and thaw cycle on methane fluxes were explicitly modeled. Wetland extent and water table fluctuations were dynamically estimated using the TOPMODEL approach that takes microtopography information into account. The model was then used to estimate the methane dynamics in the Yukon River basin from 1986 to 2005. Finally, the relationships between methane dynamics and environmental factors were analyzed.

2. Methods

2.1. Study Region and Models

[5] Our study area is the Yukon River basin in the State of Alaska (Figure 1). The Yukon River basin is the fourth largest basin in North America with a drainage area of 832,700 km^2, of which 508,900 km^2 is in Alaska. The flat coastal and river plains are characterized by a polar climate, while the interior region is dominated by subpolar conditions. Vegetation is largely dominated by boreal forest, while upland regions are usually covered by tundra (see Figure S1 in Text S1 in the auxiliary material).[1] Most of the study region is underlain with permafrost. According to the permafrost and ground-ice content data [*Brown et al.*, 2001], the permafrost in the study region was categorized into five types (Figure 1): continuous permafrost with high, medium and low ice content, which accounts for 1.22%, 17.16% and 11.59% of the total permafrost in the study region, respectively, and discontinuous permafrost with medium and low ice content, which accounts for 36.34% and 33.62%, respectively.

[6] We coupled the variable infiltration capacity (VIC) [*Liang et al.*, 1994] macroscale hydrology model with our methane emission model [*Zhuang et al.*, 2004]. The VIC model has a frozen soil algorithm [*Cherkauer and Lettenmaier*, 1999, 2003; *Cherkauer et al.*, 2003] and is suitable for cold region studies [*Su et al.*, 2005]. The VIC model can estimate water and energy balances including the

[1] Auxiliary materials are available in the HTML. doi:10.1029/2011JG001843.

freezing and thawing fronts, soil moisture and soil temperature. The methane model estimates CH_4 production (methanogenesis) that occurs in the saturated zone, and oxidation (methanotrophy) in the unsaturated zone, at an hourly time step. Methane emissions to the atmosphere are mechanistically represented with three different pathways including diffusion, plant-aided transport, and ebullition [*Zhuang et al.*, 2004]. The model considers the effect of climate, carbon substrate availability, vegetation type, root depth, soil texture, pH and redox potentials on methanogenesis and methanotrophy processes. The parameters related to those processes were also developed for main ecosystem types at northern high latitudes [e.g., *Zhuang et al.*, 2004, 2007]. In this study, we used most of the original functions and parameters describing methane production, oxidation and transport, but we improved the model in several aspects: (1) including sub-grid topographic information into water table modeling; (2) using the VIC model and the finite volume method (FVM) to model the effects of freeze/thaw cycles on methane dynamics; and (3) using a dynamic threshold for methane ebullition modeling.

2.2. Modeling Water Table Depth

[7] By using the method of *Letts et al.* [2000], the VIC model provides a grid-cell-mean water table depth based on soil moisture content in different layers. However, *Bohn and Lettenmaier* [2010] demonstrated that the average water table scheme, without considering the sub-grid variability, led to system biases in methane estimation. Therefore, we used the TOPMODEL-based formulation (equation (1)) [*Beven and Kirkby*, 1979] to represent the spatially distributed WTD for each 1*1 km pixel:

$$Z_{WTi} = Z_{WT} - f*(K_i - \lambda) \quad (1)$$

Where f is the decay parameter (meter), K_i is the topographic wetness index (TWI) and λ is the average of K_i over one specific watershed. Z_{WT} is the average WTD that is calculated from the VIC model and Z_{WTi} is the local water table depth with a spatial resolution of 1 km in this study. The WTD for each watershed is equal to the area-weighted WTD of intersected VIC grids whose WTD is provided by VIC. Moreover, *Fan and Macho* [2010] showed that the decay parameter (f) used in the TOPMODEL formulation is determined by not only terrain slope but also winter temperature if the study region is in high-latitude areas. The decay parameter is thus modeled as:

$$f = \frac{100}{1 + 150*S}(C_T) \quad (2a)$$

$$C_T = 1.5 + 0.1T \ (-14^\circ C < T < -5^\circ C, C_T < 1) \quad (2b)$$

$$C_T = 0.17 + 0.005T \ (T < -14^\circ C, C_T > 0.05) \quad (2c)$$

Where s is terrain slope, T is mean surface air temperature (Celsius) in January and C_T is a temperature modifier which makes equation (2a) more suitable in arctic regions. The f value derived from equation (2a) must be larger than 2.5. Thus, f will be set as 2.5 if equation (2a) gives values smaller than 2.5 (see Figure S2 in Text S1). The topographic information is derived from the Advanced Spaceborne Thermal Emission and Reflection Radiometer (ASTER) imagery [*Toutin*, 2002], which provides elevation data at a 30 m resolution. The TWI map for the Yukon River basin is shown in Figure S3 (in Text S1). In this study, the watershed-scale and 1*1 km local TWI used in equation 1 are the average values for the corresponding areas. To get the watershed-scale WTD, we separated the whole Yukon River basin into 722 watersheds according to the HUC10 data set from National Hydrological Data sets (NHD) (Figure 1).

2.3. Modeling Freeze and Thaw Cycles

[8] Under the VIC framework, *Cherkauer and Lettenmaier* [1999] developed a finite difference soil thermal algorithm to solve soil thermal profiles at predefined nodes through the soil column and depths of freezing and thawing fronts. The active layer is the ground layer above permafrost that is subject to summer thawing and winter refreezing. The development of these two fronts, together with change in water table depth, allows a more adequate estimation of methane emissions in high latitudes. [*Zhuang et al.*, 2003b] have also indicated that ALD could be significantly overestimated if thawing/freezing fronts are not considered, which will result in the overestimation of methane production and emissions.

[9] According to different combinations of freezing and thawing fronts and water table location, we consider six scenarios, referred to here as S1–S6 (Figure 2). The transition between seasonally frozen and non-frozen conditions coincides with abrupt changes in ALD and water phases in soils. In frozen soils, it is assumed that only methane oxidation occurs, although the contribution is small. These scenarios have different behaviors in terms of boundary conditions, methane production and oxidation.

[10] The most complicated situations occur in S1 and S2 (Figure 2), both of which have freezing and thawing fronts and water table changes. S1 represents a large regional thawing process, usually beginning in May or June, followed by a brief refreezing period, whereas the S2, frequently occurs in September and October, with a freezing trend and some thawing fluctuations. Each of them can be further classified into three subtypes according to depths of freezing and thawing fronts and water table. We found that the scenarios S2.a, S2.b, and S2.c only account for 0.007%, 0.037%, and 0.65% of all daily thawing and freezing situations in the region during the simulation period, respectively. The rare occurrence of the S2 scenario is consistent with the steadily decreasing trend of winter air temperature in our study regions. To simplify the calculation, the thawing front in S2 could be ignored. Therefore, S2 is equivalent to S3. In contrast, S1 takes 8.1% of the total simulated freezing and thawing events, and is kept in the simulation.

[11] In S1, the active layer is sandwiched between a freezing layer and permafrost. As for the sub-zone S1.a, the liquid saturated zone is the region spanning from the freezing front to the thawing front. The sub-zone S1.b has unsaturated and saturated zones separated by a water table and its lower boundary is the thawing front. The sub-zone S1.c has a water table below the thawing front; thus, there is no liquid saturated zone in the soil profile and only slow methane oxidation may occur.

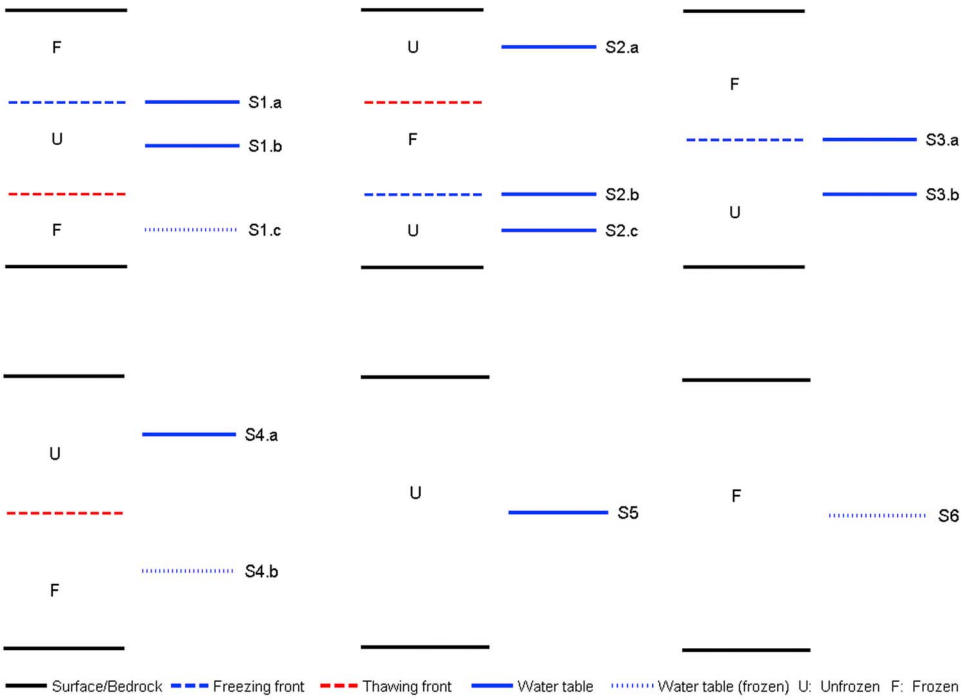

Figure 2. One-dimensional freeze/thaw scenarios considered in the methane estimation. See more detailed analysis in the text.

[12] S3 and S4 only have one freezing and thawing front, respectively (Figure 2). Each of them could be further categorized into two subtypes according to the water table depth. In S3.a, the freezing front has the same depth as the liquid water table depth, and the lower zone from the water table to the bedrock is saturated. As for S3.b, the oxidation region is between the surface and water table and a saturated zone is between the water table and the bedrock.

[13] In sub-zone S4.a, the thawing front separates the unfrozen and frozen zones. The water table separates unsaturated and saturated zones. In subzone S4.b, there is no liquid water table, thus only slight methane oxidation exists from surface to water table (frozen).

[14] S5 has a completely thawed soil profile. In this situation, methane oxidation occurs in the unsaturated zone located above the water table, while the saturated zone from the water table to the bedrock produces methane. In contrast, soils under S6 are completely frozen and there is minimum methane production and slight methane oxidation. The computational domains, boundary conditions, saturated and unsaturated zones for each scenario are listed in Table 1.

2.4. Modeling Ebullition

[15] The ebullition threshold was set as a fixed value of 500 μmol in our previous methane simulations [e.g., *Zhuang et al.*, 2004]. Here, we revised it as a function of pressure and soil temperature. According to *Yamamoto et al.* [1976], the relationship between maximum solubility of methane and temperature is fitted as:

$$S_B = 0.05708 - 0.001545*T + 0.00002069*T^2 \quad (3)$$

where S_B is the Bunsen solubility coefficient, defined as the volume of gas dissolved per volume of liquid at atmospheric

Table 1. Calculation Domain and Methane Oxidation/Production Zones in the FVM[a]

Scenarios	Calculation Domain (Upper / Lower)	Methane Oxidation Zone (Upper / Lower)	Methane Production Zone (Upper / Lower)
S1.a	surface / thawing front	surface / freezing front	freezing front / thawing front
S1.b	surface / thawing front	surface / water table	water table / thawing front
S1.c	surface / water table (frozen)	surface / water table (frozen)	NA
S3.a	surface / bedrock	surface freezing front	freezing front / bedrock
S3.b	surface / bedrock	surface / water table	water table / bedrock
S4.a	surface / thawing front	surface / water table	water table / thawing front
S4.b	surface / water table (frozen)	surface / water table (frozen)	NA
S5	surface / bedrock	surface / water table	water table / bedrock
S6	surface / water table	surface / water table	NA

[a]The atmospheric methane concentrations (0.076 μmol L^{-1}) are used for the upper boundary condition, and zero methane fluxes are assumed for the lower boundary condition.

pressure and a given temperature. T is soil temperature in Celsius. The ideal gas law is then used to convert the volume of methane per volume of water into moles as:

$$n = \frac{pV}{RT} \tag{4}$$

where $p = p_{atm} + \rho gz$ is the sum of the atmospheric and hydrostatic pressures (Pa), z is the water height (meter), V is the methane volume (m^3), T is soil temperature in Kelvin (K), the gas constant R is 8.3145 $J \cdot K^{-1} \cdot mol^{-1}$ and n is the amount of gas (mol). The ebullition is calculated for each 1 cm of the soil layer under the water table. Ebullition events occur in the layer whose methane concentration exceeds the methane maximum solubility.

2.5. Modeling Methane Fluxes

[16] We used the one-dimensional finite volume method (FVM) to solve the methane diffusion equation [*Zhuang et al.*, 2004]:

$$\frac{\partial C_M(z,t)}{\partial t} = M_p(z,t) - M_o(z,t) - \frac{\partial\left(D\frac{\partial C_M(z,t)}{\partial z}\right)}{\partial z} - R_p(z,t) - R_E(z,t) \tag{5}$$

Where $C_M(z, t)$is the soil CH_4 concentration in μmol L^{-1} at depth z (centimeters) and time t (time step = 1 h); $M_p(z, t)$, $M_o(z, t)$, $R_p(z, t)$ and $R_E(z, t)$ are the CH_4 production, oxidation, and the plant-aided and ebullition rates, respectively; z is negative when it is above the soil surface; the item $\partial(D(\partial C_M(z, t)/\partial z))/\partial z$ represents methane diffusion and D is the diffusivity (see also Text S1). In the one-dimensional FVM, the above equation is solved numerically in the computational domain and divided into a number of nodes with 1 cm for each node. Mathematically, methane production in saturated zones is treated as the source item in the FVM, and the sink terms include methane oxidation and methane transport by plants and ebullition. If there is a water table (unfrozen) in the soil column, bubbles are assumed to break out there and methane in bubbles is added at the node right above the water table. When the water table (unfrozen) is at or above the soil surface, the gases carried in the bubbles are directly emitted to the atmosphere. The trapped methane in frozen soil zones is excluded in diffusion and oxidation processes and will return to the calculation when ice layers melt. We solved the equation iteratively until methane concentrations in the soil profile are stabilized within each time step. Details of the FVM are referred to *Patankar* [1980].

3. Regional Simulations

[17] We used spatially explicit data of land cover, soils, and daily climate from a variety of sources to run the VIC model and the revised methane model. The VIC model version 4.1.1 was used to solve the moisture and energy balances at a daily time step with a spatial resolution of 30 km, and the methane model was applied at a 1 km by 1 km spatial resolution and at an hourly time step for the Yukon River basin from 1986 to 2005 (see also the VIC validation section in the Text S2). The required soil moisture, temperature and freezing/thawing fronts for estimating methane emissions are acquired from the interpolated 30*30 km VIC simulation grid.

[18] To run the VIC simulations, the model was forced by gridded daily precipitation, maximum and minimum temperatures (Tmax and Tmin) and wind speed acquired from ArcticRIMS (http://RIMS.unh.edu). The vegetation map was obtained from the University of Maryland's (UMD) 1 km Global Land Cover product [*Hansen et al.*, 2000]. Soil parameters [*Nijssen et al.*, 2001a, 2001b] and other vegetation parameters such as minimum stomatal resistance, albedo, and rooting depth and fraction specified for each individual vegetation class were obtained from the VIC model website (http://www.hydro.washington.edu/Lettenmaier/Models/VIC/).

[19] The data used for driving the methane model include monthly net primary production (NPP), a vegetation map [*Melillo et al.*, 1993], soil texture [*Zhuang et al.*, 2003b], and soil-water pH [*Carter and Scholes*, 2000]. The monthly NPP was produced by TEM. The vegetation and soil texture data sets are used to assign vegetation-specific and texture-specific parameters to a grid cell. The soil-water pH data are used to estimate methanogenesis across the study region.

[20] We evaluated the water table depth and methane emissions with observation data (Table S1, Text S2). The water table depth data were compiled from the U.S. Geological Survey (USGS) database (http://nwis.waterdata.usgs.gov/usa/nwis/gwlevels). We limited our analysis to the sites within 2 m of the land surface. The water table observations at three sites (see Figure S1[7] in Text S2) were comparable with the simulated water table dynamics. The simulated methane emissions were comparable with observed CH_4 flux data in 2004 [*Myers-Smith*, 2005]. One outlier occurred on 28 May 2004 when the observation CH_4 flux is significantly higher than the modeled value (see Table S1 in Text S2). The accumulated methane under the ice layer is most likely the reason for this discrepancy, while the pulse release due to the accumulated high concentrations has not been modeled in this study.

4. Results and Discussion

4.1. Site-Level Methane Dynamics

[21] The water table depth for the verification site (the single cylinder on the left) and its watershed (the light blue layer) on 2 August 2004 are shown in Figure 3. The light yellow and khaki layers represent surface and bedrock, respectively. The topographic wetness index (TWI) map is also shown on the top. The red and blue cylinders stand for the unsaturated and saturated zones for each pixel. The average water table depth for the watershed is different from the pixel-level water table distribution, which is more influenced by the topography. The TWI of the watershed (HUC10 1904050715) is relatively high in the middle regions of this watershed. Consequently, the water tables are shallower than those in the rest of the region.

[22] The above pixel was further used to analyze the effects of thawing/freezing fronts and water table depth on its methane dynamics. The topographic index for this pixel is 19.336 and the watershed average TWI is 14.804, which partially explains the relatively shallow local water table depth. The average January air temperature is −21°C, and the soil started to thaw on May 23 in 2004. With the

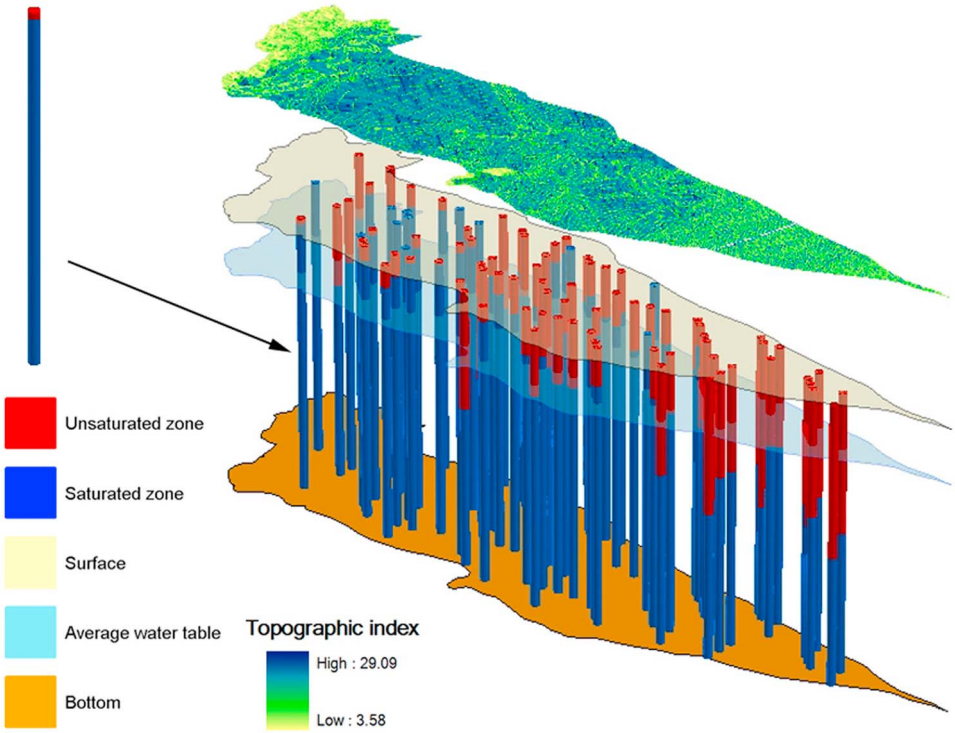

Figure 3. Water table distribution for the validation site and its watershed on August 2, 2004. Not all pixels are shown so the different layers can be more easily distinguished.

increasing soil temperature in the summer, a larger area of the soil region thawed, and thus methane production zone increased with time. The methane flux on June 14 is 12.9 mg day^{-1} m^{-2} and the methane concentration is low in soil profiles except for a higher region in the bottom (Figure 4a). Note that the thawing front is 63 cm (not shown) and 84 cm on 13 and 14 June, respectively. Therefore, we assume that the release of trapped methane during soil thawing is the reason for the high concentration in that region. On 25 July and 20 August we see typical methane dynamics for summer wetlands, where the soil profile is almost saturated and the methane flux is relatively high due to the high soil temperature and flourishing vegetation growth (Figures 4b and 4c). From the concentration profile, it is shown that the soil layer between 10 and 30 cm usually has high concentration zones where rooting systems mainly distribute.

[23] Methane flux is high (100.8 mg day^{-1} m^2) on 19 October 2004 (Figure 4d). This may be due to the dynamics of the associated water table depth and freezing front, which are 6 cm and 26 cm, respectively. The methane flux peak during the freeze-in period is also reported by other studies [*Mastepanov et al.*, 2008]. The high methane concentration zones are different on 20 August and 19 October. Specifically, high concentrations occur in upper 30 cm in summer as we mentioned above, which occur in the deeper zone between 40 and 50 cm, or even 60 cm, in the freeze-in period. The lower consumption should be one reason for the development of deeper high-concentration zones. High concentrations and low oxidation lead to peaks in methane fluxes during freeze-in periods. The freeze-in process actually creates a direct low-loss 'tube' to high methane concentration zones, while those peaks usually occur within only a few days because most of the methane production zone will be frozen in a short time. From November to the following May the whole soil profile is frozen, and low methane diffusion from atmosphere to soils will occur.

4.2. Regional Methane Emissions

[24] Our simulation estimates that the Yukon River basin emitted 4.01 Tg CH_4 yr^{-1} and there was a large interannual variability of this source during the study period (Figure 5a). Previous studies [e.g., *Dlugokencky et al.*, 2001; *Zhuang et al.*, 2004] partially attributed positive anomalies to warm conditions in the northern high latitudes due to the strong El Niño phenomena. Our simulation results support this interpretation and indicate that the region released more CH_4 in 1998, an amount that is 0.5–2 Tg CH_4 higher than the emissions in 1997 and 1999. In contrast, the region showed a significant decrease in net CH_4 emissions in 1995, 1996 and 1999 when there were strong La Niña phenomena. Recently, *Hodson et al.* [2011] suggested El Niño phases may lead to larger negative CH_4 anomalies and there is a positive trend in La Niña years by correlating methane emissions from a simple wetland model with an ENSO index. The discrepancy may be due to the fact that: (1) our study is focused on the Yukon River basin, while the relationship proposed by Hodson *et al.* is on the global scale, and (2) the Hodson study did not consider temperature as an important indicator of CH_4 variability at higher latitudes. The methane source strength varies over the Yukon River basin and large regions have actually been small net sinks of atmospheric CH_4 (Figure 6). Figure S4 in Text S1 shows the frequency distribution of nonzero values in Figure 6. Most of pixels have

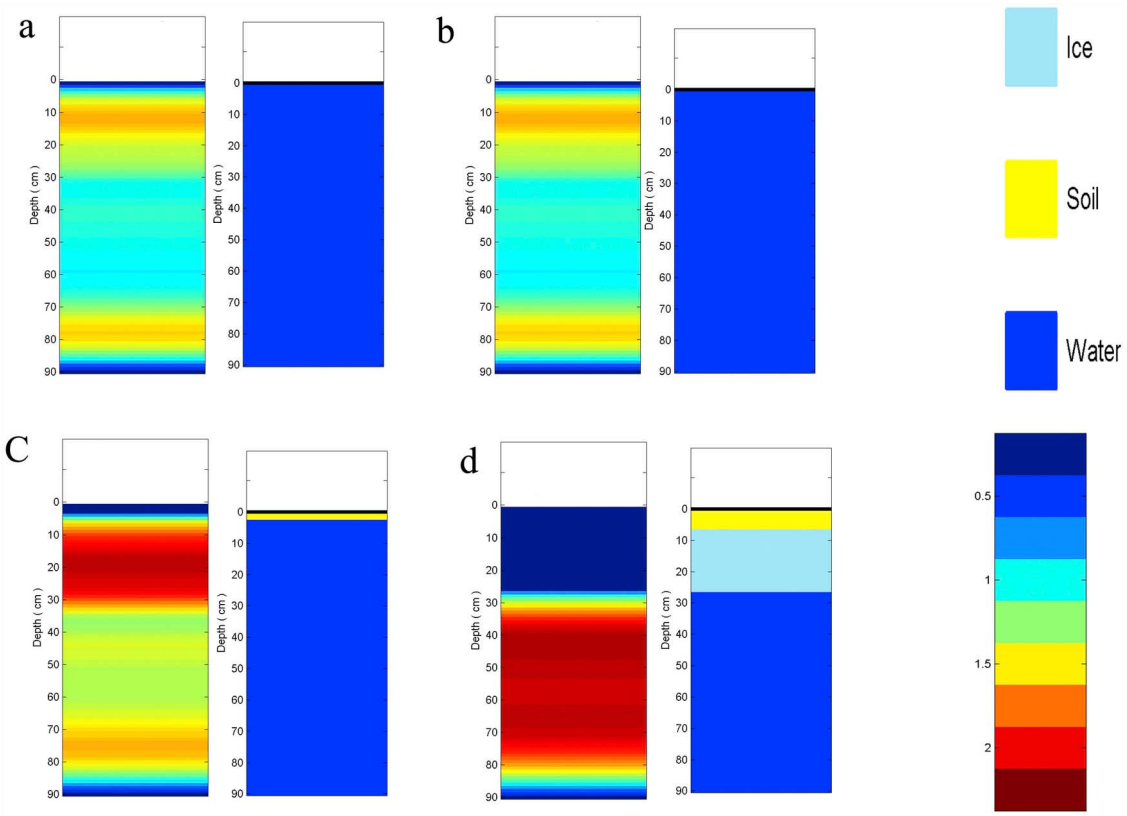

Figure 4. Methane concentration profiles and soil moisture conditions for the validation site on (a) 4 June 2004, (b) 7–25 June 2004, (c) 8–20 June 2004, and (d) 10–19 June 2004, respectively. The methane concentration units are μmol/cm^3. See more explanation in the text.

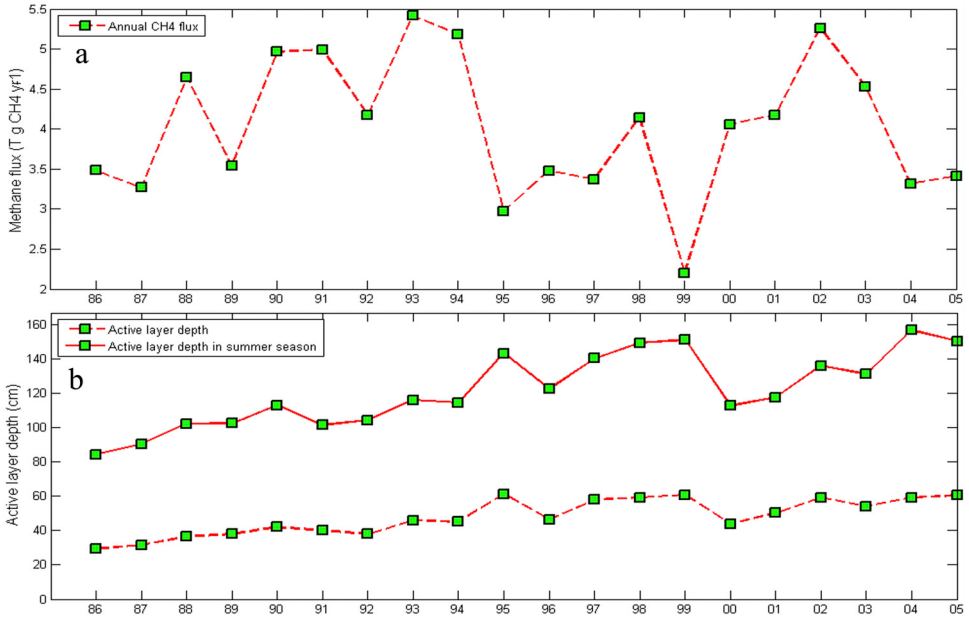

Figure 5. The annual dynamic of (a) methane flux and (b) active layer depth in the Yukon River basin, 1986–2005.

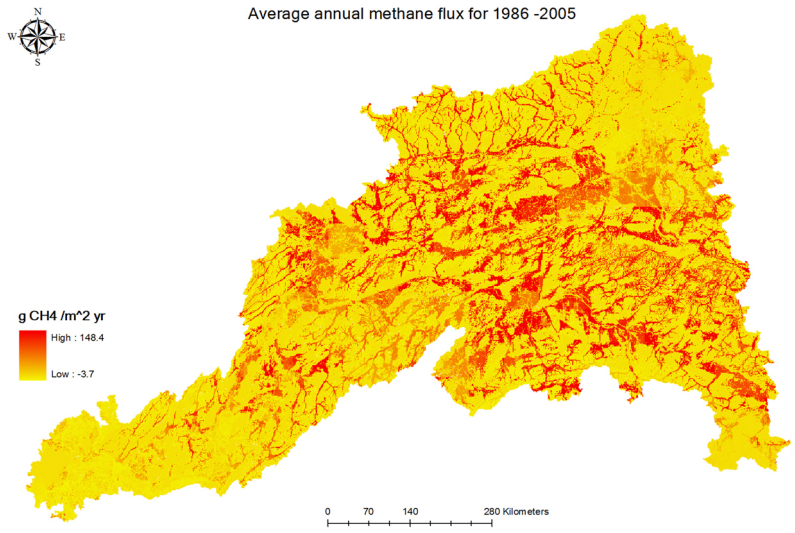

Figure 6. Average annual methane fluxes (g CH_4 m^{-2} yr^{-1}) in the Yukon River basin, 1986–2005. Positive values are emissions and negative values are oxidation.

very low or even slight negative methane emission values. Pixels with more than 60 g CH_4 m^{-2} yr^{-1} only account for 1.5% of the total number of pixels. Water table depth is the fundamental factor deciding whether a pixel is a methane sink or source. For pixels with a water table depth more than 30 cm, methane produced in the saturated zone can be almost completely oxidized within unsaturated regions. In our simulations, lowlands, such as valleys, and areas near rivers and wetlands, act as a relatively strong CH_4 source.

[25] Regional daily methane emissions showed two peaks (Figure 7). The first one, known as the spring burst in some other studies [*Tokida et al.*, 2007], can be explained by the increase in saturated soil zones and the release of trapped methane, both due to ice and snowmelting. The second peak, which usually happens in late August, September and early October, may be explained by the effects of low evapotranspiration and the freeze-in process. The two peaks of methane emissions are related to the double-peak trend in the change of saturated zones, as discussed later [*Su et al.*, 2005]. In addition, July did not have as high methane emissions as those from the two peak times, although soil temperature was higher at that time. This might be due to the high oxidation and lower production induced by the relatively strong evapotranspiration and a lower water table.

4.3. Relationships Between Regional Hydrology and Methane Dynamics

[26] By assuming that woody and emergent wetlands in the NLCD 2001 are saturated zones, we estimated the area of the saturated zone to be 47218 km^2 (Figure 8a). There are high variations in the area of saturated zone, suggesting that using static wetland distribution data in methane emissions studies may introduce large biases (Figure 8b). For instance, an application of TEM for the whole of Alaska estimated the total emissions to be 3 Tg CH_4 yr^{-1} using a static wetland distribution data set [*Zhuang et al.*, 2007]. The area of saturated zones in the Yukon River basin is usually very small in the winter and early spring. It increases significantly on around the day of year (DOY) 140 and arrives at the annual peak on the DOY 180. There is a double-peak trend in the change of saturated zones. The first one usually occurs during the period of May to June, arising from spring snowmelt; the second one, which is much lower than the first, normally happens in late August and early September due to relatively high precipitation supply [*Su et al.*, 2005]. The daily methane flux time series (Figure 7 and Figure 8b) roughly mimics this double-peak pattern but with different amplitudes. Usually, the second peak is stronger than the first one. The reason is that most of the saturated zone during the spring snowmelt still has low soil temperature, and methane production is still limited.

[27] To examine the effect of topography on methane fluxes, we separated all the pixels into two groups according to their topographic index. Specifically, one group, called the higher TWI group, includes all the pixels having at least

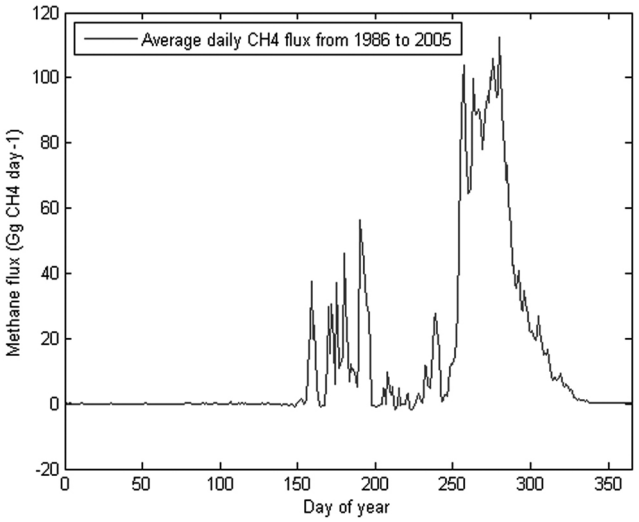

Figure 7. Average daily methane fluxes from the Yukon River basin from 1986 to 2005.

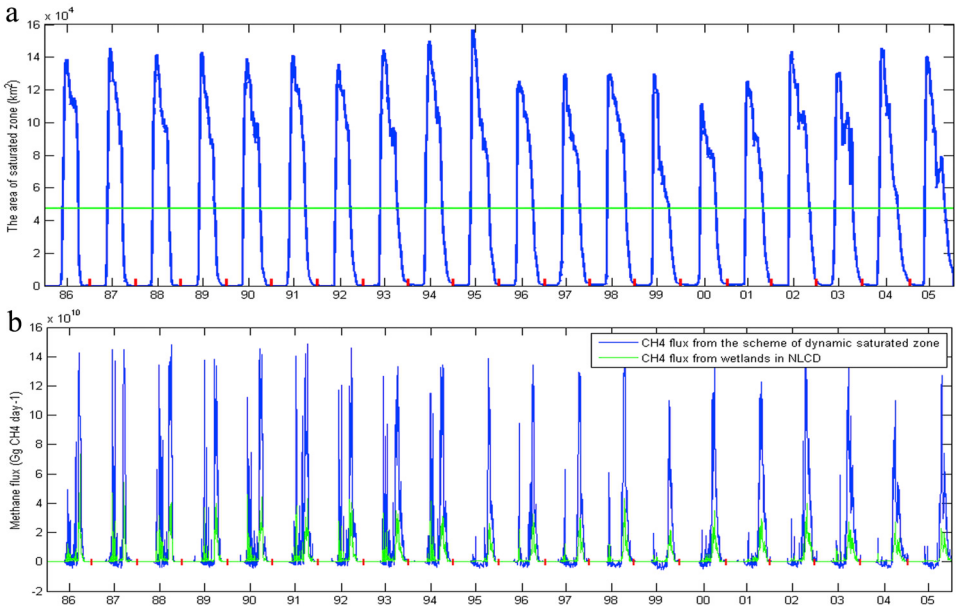

Figure 8. Daily dynamics of (a) the saturated zone and (b) methane fluxes in the Yukon River basin during 1986–2005. The green line in Figure 8a represents the saturated zone (wetlands and water bodies) in the NLCD 2001.

10% higher TWI than their own HUC10 average watershed TWI; the other group, called the lower TWI group, contained the rest of pixels. We selected data for the period from the DOY 150 to 300, when methane fluxes are usually at a high level, to do the experiment. The number of the higher TWI groups is usually only 25% of that of the lower TWI group, while the methane flux from the lower TWI group is only 40–50% of that in the higher TWI group (Figure S5 in Text S1). This suggests that topography, by redistributing soil moisture and the water table, significantly affects the total methane fluxes and their spatial distribution.

4.4. Effects of the Regional Soil Thermal Regime on Methane Dynamics

[28] Active layer depth (ALD) has deepened around 15 cm during the study period (Figure 5b). There are two sudden events: one is a significant melt in 1995 and the other is a quick freezing event in 2000. The two soil thermal events correspond to the strong ENSO events: the former one is El Niño state, while the latter is La Niña. The simulated permafrost thawing, resulting in more methane production in the soil column, is consistent with field observations in the subarctic regions [*Payette et al.*, 2004].

[29] While the increase in the thickness of the active layer is usually thought to be associated with larger CH_4 emissions, our study shows the opposite. The rooting depth distribution may be one reason for that. In our model framework, methane production is highly influenced by root exudates, which are a function of the NPP of the overlying vegetation and the rooting depth distribution. If z in $M_p(z, t)$ is below the rooting depth, substrate availability is assumed to decrease exponentially with depth. In the Yukon River basin, the main ecosystem types are assumed to usually have the rooting depth of 60–80 cm below the ground [*Zhuang et al.*, 2004] where soils usually melt in the summer season (Figure 5b). Therefore, the increase in ALD has not necessarily led to a significant increase in the simulated CH_4 emissions due to less organic carbon substrate for methane production in deeper soils.

[30] The trend of the saturated areas in the summer season and precipitation showed a pattern similar to the average annual methane fluxes (Figure S6 in Text S1; Figure 5a). Our analyses indicate that annual net CH_4 emissions are more correlated with precipitation ($R^2 = 0.84$; $P < 0.01$) than average annual soil temperature ($R^2 = 0.57$; $P < 0.01$) and ALD ($R^2 = 0.47$; $P < 0.01$). These analyses suggest that changes in climate and their influence on the soil moisture condition may be a main determinant to the dynamics of CH_4 emissions.

5. Conclusions

[31] In this study, we coupled the macro-hydrological model VIC and a process-based methane model to estimate methane emissions at a 1*1 km resolution from the Yukon River basin from 1986 to 2005. Several key soil thermal and hydrological regimes related to CH_4 emissions are explicitly modeled. Specifically, the freezing and thawing cycle, an important process in modeling methane emissions from permafrost regions, is modeled with the VIC model. We showed that a large methane burst during freeze-in periods is due to frozen low-loss tubes in high methane concentration zones in the soil profile. Our study suggests that static wetland distribution data or satellite data with a low time resolution are not sufficient for estimating methane emissions. The expansion and contraction of wetlands are affected by local topography. To take this sub-grid topography variability into account, the TOPMODEL approach was used to redistribute watershed average water table depth, simulated with the VIC model, into finer grids. We found that average

annual net emissions of CH_4 is 4.01 Tg CH_4 yr^{-1} and has large seasonal variation. By considering the fact that our study region accounts for around 2% of total area of boreal/arctic land, we noted that our estimation is more than 3 times higher than most estimates for northern wetlands in the same region [*McGuire et al.*, 2009; *Mikaloff Fletcher et al.*, 2004]. We believe the difference in our estimate relative to the estimates generated by previous studies can be primarily explained by these three reasons: (1) the method in this study is different from previous studies. We tried to capture detailed topography information within relative large simulation grid. As we mentioned above, methods without considering sub-grid variations in water table may introduce quite large biases into methane emission estimation, (2) saturated zones are updated at each time step in this study, while many other studies assume a static wetland distribution and (3) our parameters, such as soil depth, hydraulic conductivity, thermal conductivity are different from other studies. During the study period, the region had a general increasing trend in net CH_4 emissions. Air temperature explains most of the CH_4 variability in this region. ENSO variability is strongly linked to the CH_4 interannual variability. More CH_4 is emitted in El Niño events than in La Niña events in the region.

[32] **Acknowledgments.** This study was supported through projects funded to Qianlai Zhuang by the NSF Carbon and Water in the Earth Program (EAR-0630319), the NASA Land Use and Land Cover Change Program (NASA-NNX09AI26G), the U.S. Department of Energy (DE-FG02-08ER64599), and the NSF Division of Information and Intelligent Systems (NSF-1028291). We thank Dr. Keith Beven of Lancaster University, who provided TOPMODEL algorithm code. We thank Ian Pope and Jaye Piepenbug for help checking the English grammar. Computing support was provided by the Rosen Center for Advanced Computing (RCAC) at Purdue University.

References

Aselmann, I., and P. J. Crutzen (1989), Global distribution of natural freshwater wetlands and rice paddies, and their net primary productivity, seasonality and possible methane emissions, *J. Atmos. Chem.*, *8*, 307–358, doi:10.1007/BF00052709.

Beven, K. J., and M. J. Kirkby (1979), A physically based, variable contributing area model of basin hydrology, *Hydrol. Sci. Bull.*, *24*, 43–69, doi:10.1080/02626667909491834.

Bohn, T. J., and D. P. Lettenmaier (2010), Systematic biases in large-scale estimates of wetland methane emissions arising from water table formulations, *Geophys. Res. Lett.*, *37*, L22401, doi:10.1029/2010GL045450.

Bohn, T. J., D. P. Lettenmaier, K. Sathulur, L. C. Bowling, E. Podest, K. C. McDonald, and T. Friborg (2007), Methane emissions from western Siberian wetlands: Heterogeneity and sensitivity to climate change, *Environ. Res. Lett.*, *2*, 045015, doi:10.1088/1748-9326/2/4/045015.

Brown, J., O. J. Ferrians, J. A. Heginbottom, and E. S. Melnikov (2001), Circum-Arctic map of permafrost and ground-ice conditions, digital map, Natl. Snow and Ice Data Cent./World Data Cent. for Glaciol., Boulder, Colo. [Available at http://nsidc.org/data/ggd318.html.]

Carter, A. J., and R. J. Scholes (2000), *SoilData v2.0: Generating a Global Database of Soil Properties*, Counc. for Sci. and Ind. Res. Environ., Pretoria, South Africa.

Cherkauer, K. A., and D. P. Lettenmaier (1999), Hydrologic effects of frozen soils in the upper Mississippi River basin, *J. Geophys. Res.*, *104*(D16), 19,599–19,610, doi:10.1029/1999JD900337.

Cherkauer, K. A., and D. P. Lettenmaier (2003), Simulation of spatial variability in snow and frozen soil, *J. Geophys. Res.*, *108*(D22), 8858, doi:10.1029/2003JD003575.

Cherkauer, K. A., L. C. Bowling, and D. P. Lettenmaier (2003), Variable infiltration capacity cold land process model updates, *Global Planet. Change*, *38*(1–2), 151–159, doi:10.1016/S0921-8181(03)00025-0.

Dlugokencky, E. J., B. P. Walter, K. A. Masarie, P. M. Lang, and E. S. Kasischke (2001), Measurements of an anomalous global methane increase during 1998, *Geophys. Res. Lett.*, *28*(3), 499–502, doi:10.1029/2000GL012119.

Fan, Y., and G. M. Macho (2010), A simple hydrologic framework for simulating wetlands in climate and earth system models, *Clim. Dyn.*, *37*, 253–278, doi:10.1007/s00382-010-0829-8.

Hansen, M. C., R. S. DeFries, J. R. G. Townshend, and R. Sohlberg (2000), Global land cover classification at 1 km resolution using a classification tree approach, *Int. J. Remote Sens.*, *21*, 1331–1364, doi:10.1080/014311600210209.

Hodson, E. L., B. Poulter, N. E. Zimmermann, C. Prigent, and J. O. Kaplan (2011), The El Niño–Southern Oscillation and wetland methane interannual variability, *Geophys. Res. Lett.*, *38*, L08810, doi:10.1029/2011GL046861.

Intergovernmental Panel on Climate Change (2007), *Climate Change: Synthesis Report: Contribution of Working Groups I, II, and III to the Fourth Assessment Report of the Intergovernmental Panel on Climate Change*, 104 pp., IPCC, Geneva, Switzerland.

Khvorostyanov, D. V., P. Ciais, G. Krinner, and S. A. Zimov (2008), Vulnerability of east Siberia's frozen carbon stores to future warming, *Geophys. Res. Lett.*, *35*, L10703, doi:10.1029/2008GL033639.

Letts, M. G., N. T. Roulet, N. T. Comer, M. R. Skarupa, and D. Verseghy (2000), Parameterization of peatland hydraulic properties for the Canadian Land Surface Scheme, *Atmos. Ocean*, *38*, 141–160, doi:10.1080/07055900.2000.9649643.

Liang, X., D. P. Lettenmaier, E. Wood, and S. Burges (1994), A simple hydrologically based model of land surface water and energy fluxes for general circulation models, *J. Geophys. Res.*, *99*(D7), 14,415–14,428, doi:10.1029/94JD00483.

Mastepanov, M., S. Charlotte, E. J. Dlugokencky, H. Sander, S. Lena, P. T. Mikkel, and R. C. Torben (2008), Large tundra methane burst during onset of freezing, *Nature*, *456*, 628–630, doi:10.1038/nature07464.

Matthews, E., and I. Fung (1987), Methane emissions from natural wetlands: Global distribution, area, and environmental characteristics of sources, *Global Biogeochem. Cycles*, *1*(1), 61–86, doi:10.1029/GB001i001p00061.

McGuire, A. D., L. G. Anderson, T. R. Christensen, S. Dallimore, L. D. Guo, D. J. Hayes, M. Heimann, T. D. Lorenson, R. W. Macdonald, and N. Roulet (2009), Sensitivity of the carbon cycle in the Arctic to climate change, *Ecol. Monogr.*, *79*, 523–555, doi:10.1890/08-2025.1.

Melack, J. M., L. L. Hess, M. Gastil, B. R. Forsberg, S. K. Hamilton, I. B. T. Lima, and E. M. L. M. Novo (2004), Regionalization of methane emissions in the Amazon Basin with microwave remote sensing, *Global Change Biol.*, *10*, 530–544, doi:10.1111/j.1365-2486.2004.00763.x.

Melillo, J. M., A. D. McGuire, D. W. Kicklighter, B. Moore III, C. J. Vörösmarty, and A. L. Schloss (1993), Global climate change and terrestrial net primary production, *Nature*, *363*, 234–240, doi:10.1038/363234a0.

Mikaloff Fletcher, S. E., P. P. Tans, L. M. Bruhwiler, J. B. Miller, and M. Heimann (2004), CH_4 sources estimated from atmospheric observations of CH_4 and its $^{13}C/^{12}C$ isotopic ratios: 2. Inverse modeling of CH_4 fluxes from geographical regions, *Global Biogeochem. Cycles*, *18*, GB4005, doi:10.1029/2004GB002224.

Myers-Smith, I. H. (2005), Carbon exchange and permafrost collapse: Implications for a changing climate, MS thesis, Univ. of Alaska Fairbanks, Fairbanks, Alaska.

Nijssen, B., G. M. O'Donnell, D. P. Lettenmaier, D. Lohmann, and E. F. Wood (2001a), Predicting the discharge of global rivers, *J. Clim.*, *14*, 3307–3323, doi:10.1175/1520-0442(2001)014<3307:PTDOGR>2.0.CO;2.

Nijssen, B., G. M. O'Donnell, A. F. Hamlet, and D. P. Lettenmaier (2001b), Hydrologic sensitivity of global rivers to climate change, *Clim. Change*, *50*, 143–175, doi:10.1023/A:1010616428763.

O'Connor, F. M., et al. (2010), Possible role of wetlands, permafrost, and methane hydrates in the methane cycle under future climate change: A review, *Rev. Geophys.*, *48*, RG4005, doi:10.1029/2010RG000326.

Papa, F., C. Prigent, B. Legresy, and F. Rémy (2006), Inundated wetland dynamics from remote sensing: Using Topex-Poseidon dual-frequency radar altimeter observations over boreal regions, *Int. J. Remote Sens.*, *27*, 4847–4866, doi:10.1080/01431160600675887.

Patankar, S. V. (1980), *Numerical Heat Transfer and Fluid Flow*, *Comput. Methods Mech. Thermal Sci. Ser.*, Hemisphere, New York.

Payette, S., A. Delwaide, M. Caccianiga, and M. Beauchemin (2004), Accelerated thawing of subarctic peatland permafrost over the last 50 years, *Geophys. Res. Lett.*, *31*, L18208, doi:10.1029/2004GL020358.

Prigent, C., F. Papa, F. Aires, W. B. Rossow, and E. Matthews (2007), Global inundation dynamics inferred from multiple satellite observations, *J. Geophys. Res.*, *112*, D12107, doi:10.1029/2006JD007847.

Su, F. G., J. C. Adam, L. C. Bowling, and D. P. Lettenmaier (2005), Streamflow simulations of the terrestrial Arctic domain, *J. Geophys. Res.*, *110*, D08112, doi:10.1029/2004JD005518.

Tokida, T., M. Mizoguchi, T. Miyazaki, A. Kagemoto, O. Nagata, and R. Hatano (2007), Episodic release of methane bubbles from peatland

during spring thaw, *Chemosphere*, *70*(2), 165–171, doi:10.1016/j.chemosphere.2007.06.042.

Toutin, T. (2002), Three-dimensional topographic mapping with ASTER stereo data in rugged topography, *IEEE Trans. Geosci. Remote Sens.*, *40*(10), 2241–2247, doi:10.1109/TGRS.2002.802878.

Walter, B. P., M. Heimann, and E. Matthews (2001), Modeling modern methane emissions from natural wetlands: 2. Interannual variations 1982–1993, *J. Geophys. Res.*, *106*(D24), 34,207–34,219, doi:10.1029/2001JD900164.

Wania, R., I. Ross, and I. C. Prentice (2010), Implementation and evaluation of a new methane model within a dynamic global vegetation model: LPJ-WHyMe v1.3, *Geosci. Model Dev. Discuss.*, *3*(1), 1–59, doi:10.5194/gmdd-3-1-2010.

Yamamoto, S., J. B. Alcauskas, and T. E. Crozier (1976), Solubility of methane in distilled water and seawater, *J. Chem. Eng. Data*, *21*(1), 78, doi:10.1021/je60068a029.

Zhuang, Q., V. E. Romanovsky, and A. D. McGuire (2001), Incorporation of a permafrost model into a large-scale ecosystem model: Evaluation of temporal and spatial scaling issues in simulating soil thermal dynamics, *J. Geophys. Res.*, *106*(D24), 33,649–33,670, doi:10.1029/2001JD900151.

Zhuang, Q., A. D. McGuire, J. Harden, K. P. O'Neill, V. E. Romanovsky, and J. Yarie (2003a), Modeling soil thermal and carbon dynamics of a fire chronosequence in interior Alaska, *J. Geophys. Res.*, *108*(D1), 8147, doi:10.1029/2001JD001244.

Zhuang, Q., et al. (2003b), Carbon cycling in extratropical terrestrial ecosystems of the Northern Hemisphere during the 20th century: A modeling analysis of the influences of soil thermal dynamics, *Tellus, Ser. B*, *55*(3), 751–776, doi:10.1034/j.1600-0889.2003.00060.x.

Zhuang, Q., J. M. Melillo, D. W. Kicklighter, R. G. Prinn, A. D. McGuire, P. A. Steudler, B. S. Felzer, and S. Hu (2004), Methane fluxes between terrestrial ecosystems and the atmosphere at northern high latitudes during the past century: A retrospective analysis with a process-based biogeochemistry model, *Global Biogeochem. Cycles*, *18*, GB3010, doi:10.1029/2004GB002239.

Zhuang, Q., J. M. Melillo, A. D. McGuire, D. W. Kicklighter, R. G. Prinn, P. A. Steudler, B. S. Felzer, and S. Hu (2007), Net emissions of CH_4 and CO_2 in Alaska: Implications for the region's greenhouse gas budget, *Ecol. Appl.*, *17*(1), 203–212, doi:10.1890/1051-0761(2007)017[0203:NEOCAC]2.0.CO;2.

X. Lu and Q. Zhuang, Department of Earth and Atmospheric Sciences, Purdue University, CIVL 550, Stadium Mall Dr., West Lafayette, IN 47907, USA.